Koltzer, N., Inbar, N., Kühn, M., Möller, P., Rosenthal, E., Schneider, M., Siebert, C., Raggad, M., Magri, F. (2016):Inverse Problem to Constrain Hydraulic and Thermal Parameters Inducing Anomalous Heat Flow in the Lower Yarmouk Gorge. - *Energy Procedia*, *97*, pp. 419—426.

DOI: http://doi.org/10.1016/j.egypro.2016.10.038

Available online at www.sciencedirect.com

ScienceDirect

Energy Procedia 97 (2016) 419 – 426

Energy Procedia

European Geosciences Union General Assembly 2016, EGU
Division Energy, Resources & Environment, ERE

Inverse problem to constrain hydraulic and thermal parameters inducing anomalous heat flow in the Lower Yarmouk Gorge

Nora Goretzki[a,b*], Nimrod Inbar[c], Michael Kühn[a], Peter Möller[a], Eliyahu Rosenthal[c], Michael Schneider[b], Christian Siebert[d], Marwan Raggad[e] and Fabien Magri[f,b]

[a]*GFZ German Research Centre for Geosciences, Section 3.4 - Fluid Systems Modelling, Potsdam, Germany*
[b]*Freie Universität Berlin, Hydrogeology, Berlin, Germany*
[c]*Tel Aviv University, TheDepartment of Geophysics and Planetary Sciences, Tel Aviv, Israel*
[d]*Helmholtz Centre for Environmental Research – UFZ, Halle, Germany*
[e]*University of Jordan, Amman, Jordan*
[f]*Helmholtz Centre for Environmental Research – UFZ, ENVINF, Leipzig,Germany*

Abstract

In the present study, inverse problems (IP) are applied with FEPEST® in FEFLOW® to find parameter distributions of hydraulic and thermal conductivity that lead to the observed thermal anomalies in the Lower Yarmouk Gorge (LYG) and a more accurate fit of borehole data. Results indicate reduced hydraulic conductivities in shallower parts of the system than previously estimated. The absence of a fault under the Lower Yarmouk Gorge in deeper sediments can be superseded by presence of interconnecting local fractures. The contribution of the conductive thermal regime turns out to be negligible.

Peer-review under responsibility of the organizing committee of the General Assembly of the European Geosciences Union (EGU)

Keywords: Inverse Problem; FEPEST; hydraulic conductivity; Lower Yarmouk Gorge, Tiberias Basin; fault; temperature anomaly

* Corresponding author. Tel.: +49 331 288-28723; fax: +49 331 288-1529.
E-mail address: goretzki@gfz-potsdam.de

Peer-review under responsibility of the organizing committee of the General Assembly of the European Geosciences Union (EGU)
doi:10.1016/j.egypro.2016.10.038

1. Introduction

Lake Tiberias (LT; Fig. 1) is located in the Tiberias Basin (TB), which is part of the Dead Sea Transform. Several brackish and saline springs characterized by elevated temperatures (up to 50 °C) and diverse chemical composition (e.g. [1]) can be found in the area. As the lake is one of the main freshwater resources of the region, it is important to understand the hydrological processes causing the upsurge of potentially polluting thermal waters. Several hydrochemical investigations [2,3] and numerical studies [4-7] showed that the faults of the TB act as major flow pathways for ascending deep fluids and meteoric waters that feed the observed springs. In this respect, the anomalously high temperature gradient of 46 °C/km measured in the Lower Yarmouk Gorge (LYG; Fig. 1) and geochemical investigations raised the question whether the gorge is also hosting a geological feature (e.g. a fault) enhancing upward heat migration [8,9].

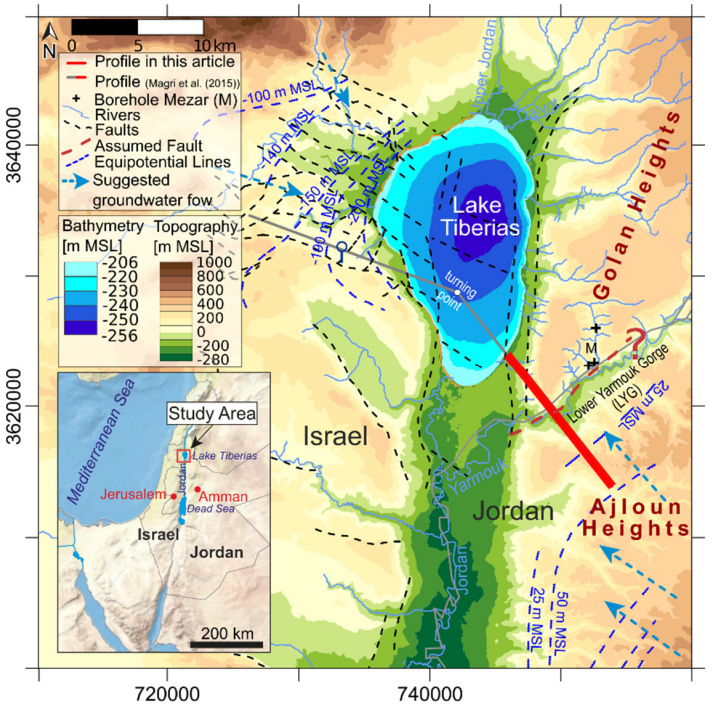

Fig. 1. Study area with topography, location of profile, faults and deep boreholes. The Tiberias Basin is situated in the northeastern part of Israel within the Jordan Rift Valley (JRV). The numerical examples of this article are based on structural features of the Lower Yarmouk Gorge (LYG), along the S-E ending of the cross-section highlighted with a bold red line. To date, the presence of a fault in the LYG is debated.

According to numerical investigations [4,7], the presence of a permeable fault or an anisotropic zone is necessary to induce buoyancy forces, locally increasing groundwater temperature in the LYG, which resemble those measured in the Meizar wells (M in Fig. 1). However, the existence of a fault in the LYG is still disputable.

In these numerical investigations, the calibration was done with a trial and error technique, i.e. several forward problems (FP) were run to perform a sensitivity analysis restricted to the faults hydraulic conductivity. However, other geological units might play an important role in controlling heat flux within the system and the assumption of homogenous faults is not supported by any crustal permeability model (e.g. [10]). Furthermore, the heat conductivity of deep units might also contribute to generate local temperature anomalies.

A useful tool to tackle the limitations of a manual calibration is inverse modelling, i.e. inverse problems (IP), which are used to identify model parameters [11,12]. Besides being an automatic approach that speeds up the

calibration process, the IP allows to cover a wide range of parameter values, providing additional solutions [13]. Examples of large-scale IP can be found in [14,15].

In this study, the inverse problem (IP) is solved with respect to (i) hydraulic conductivity (K) and (ii) thermal conductivity (λ) with the aim to infer additional parameter distributions that can reproduce the LYG thermal anomaly.

This work provides an IP in a complex hydrogeological setting, which bears high parameter uncertainties, inherent to the basin-scale of the studied processes. Hence, two scenarios are intended to reveal whether the hydraulic conductivity can be varied to better fit the temperature profile of the borehole data (scenario 1) and whether a fault along the LYG or local deep fractures cause the thermal surface anomaly (scenario 2).

2. Method

Forward and inverse modeling of coupled fluid flow and heat transport processes are carried out along a representative cross-section of the LYG (Fig. 1). The main goal is to apply IP to infer spatial distributions of hydraulic and thermal conductivities that generate the LYG thermal anomaly. The automated procedure to solve the FP/IP is summarized in Fig. 2, similar to the approach given in [16].

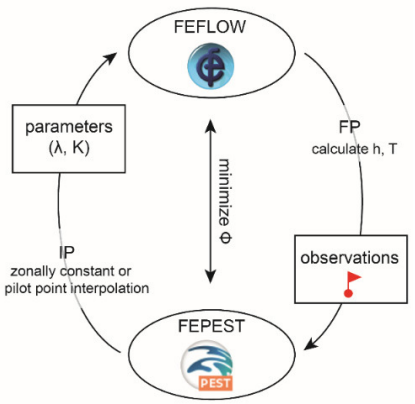

Fig. 2. The applied workflow starts by building the FP (referred to as "basic model") in FEFLOW®. The FP uses boundary conditions and parameters of the calibrated models from [1]. Hydraulic head (h) and temperature (T) are calculated. Subsequently, the estimation process of parameters (λ and K) is run with FEPEST®, in the first scenario with a zonally constant parameter distribution and in a second scenario with pilot point interpolation in the faults. The objective function (Φ) is minimized and in each iteration process, the model is run several times.

The FP are solved with FEFLOW® [17], using the finite element mesh and boundary conditions given in [4]. Mass conservation laws of momentum and heat are fully coupled through temperature dependent fluid properties. Forward and inverse problems are run under steady state conditions.

The obtained solution (head, temperature) is subsequently loaded in FEPEST®, the graphic interface of the PEST® software [18], and is used in the IP as base for the parameter estimation process. Observations are imported from FEFLOW® directly as reference values for head distributions in the upper half of the model (36 grid points, green in Fig. 3), temperature distributions around the thermal plume under the LYG (48 nodes, red in Fig. 3) and temperatures in the basement (249 nodes, blue in Fig. 3). Measured temperatures of the Meizar boreholes are also used for the calculations (four values, purple in Fig. 3). The large amount of "observation points" in the basement reflects the assumption that the Triassic sediments of the area are in a conductive thermal equilibrium.

As final check, an additional FP that uses the new set of K and λ (Fig. 2) is run in order to verify whether the calibration process provides head and temperature distributions consistent with the observations.

One challenge is that IP are in most cases ill-posed, which leads to some complications: (i) non-uniqueness, (ii) non-existence and (iii) non-steadiness [19]. The fundamental feature for optimizing the model parameters in PEST®

is the Gauss-Levenberg-Marquardt algorithm (GLMA). It iteratively adjusts the parameters in such a way that the objective function (equation 1) is minimized. The objective function is the sum of the weighted residuals squared:

$$\Phi = \sum_i w_i (h_i^{obs} - h_i^{sim})^2 \quad (1)$$

where w is the weight, i is the number of observations, and $h_i^{obs} - h_i^{sim}$ is the difference between simulated and observed data. In this work, regularization and estimation modes are used. PEST® adjusts parameter values based on the derivatives of the observations with respect to the parameters. Parameter estimation of a nonlinear problem is an iterative process, in which the objective function (Φ) is minimized and in each iteration process, the model is run several times.

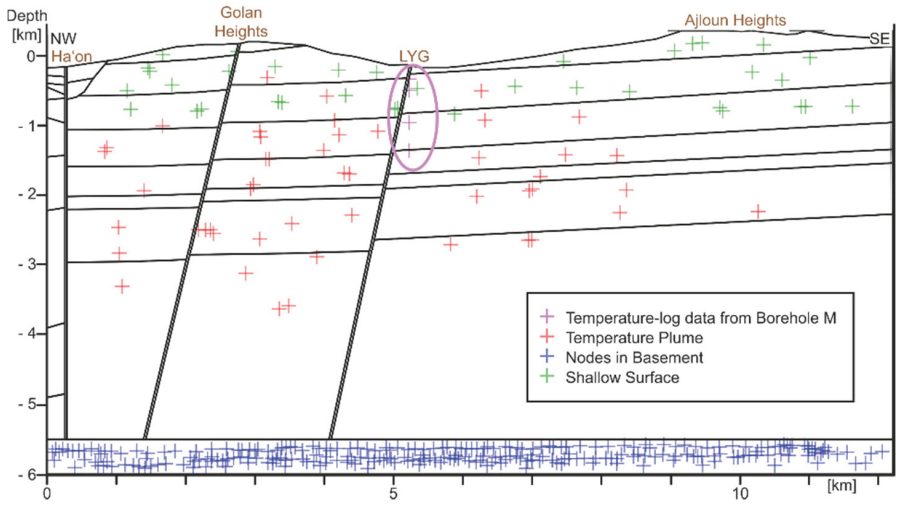

Fig. 3: Distribution of observation points across the 2D vertical profile classified in four observation point groups (green, blue, red and purple crosses). Observation points for the hydraulic heads are illustrated with green crosses, the observation point group illustrated with blue crosses defines the geothermal heat from below, the observation point group with red crosses show the temperature distribution around the thermal plume and purple crosses are observations points for temperature borehole data.

In this study, hydraulic conductivity (K) and thermal conductivity (λ) are adjusted within a given range that represents minimum and maximum values inferred from available literature. All other parameters are fixed, set equal to those of the FP, as given in Table 2.

2.1. Scenario 1

In scenario 1, hydraulic conductivity is estimated as a zonally constant parameter, where zones correspond to the stratigraphy of the profile. One value is estimated for each unit and one value for the faults. The initial values are the same as in the basic model. Units not given in Table 1 (Basement and Triassic) are fixed in this scenario with values from the base model.

2.2. Scenario 2

In scenario 2, hydraulic conductivity values in the faults are estimated via pilot points (40 pilot points in each fault) to infer a heterogeneous permeability distribution. In the surrounding units (Mi, E, SP, TS, Ce, Cr, J),

parameters are estimated zonally constant. In the Jurassic and Basement, the values are fixed. All initial values are the values from the base model.

3. Results and discussion

The basic model (FP) used to initiate the IP was calibrated manually running several FP (trial and error technique). Hydraulic conductivity values of the units and faults are adopted from [4], as listed in Table 1.

Table 1. Hydraulic conductivity (m/d) derived from FP simulations (base model) and two scenarios calibrated automatically (IP): in scenario 1, the parameters in all units and faults are zonally constant; in scenario 2, the parameters in units are zonally constant but faults heterogeneous.

Geological units (zones in FEPEST®)	Base model (FP)	Scenario 1 (IP)	Scenario 2 (IP)
Miocene Hordos (Mi)	0.01	0.01	0.02
Eocene (E)	0.03	0.03	0.04
Upper Cretaceus (Senonian Paleocene, SP)	0.003	0.001	0.001
Turonian and Senonian (TS)	0.1	0.1	0.09
Cenomanian (Ce)	0.05	0.04	0.06
Lower Cretaceous (Cr)	0.2	0.2	1
Jurassic (J)	0.06	0.02	0.01
Faults (F)	0.08	0.05	0.008– 0.2

The large-scale values indicate that the Senonian Paleocene unit acts as the main aquitard, separating shallow groundwater of the upper Miocene and Eocene aquifers from the deeper units. The hydraulic conductivities of the faults and upper aquifer (Miocene and Eocene) are in the same order of magnitude, whereas the hydraulic conductivity of the Lower Cretaceous aquifer is five times higher than calibrated within the base model.

A typical temperature profile calculated with the FP is illustrated in Fig. 4.

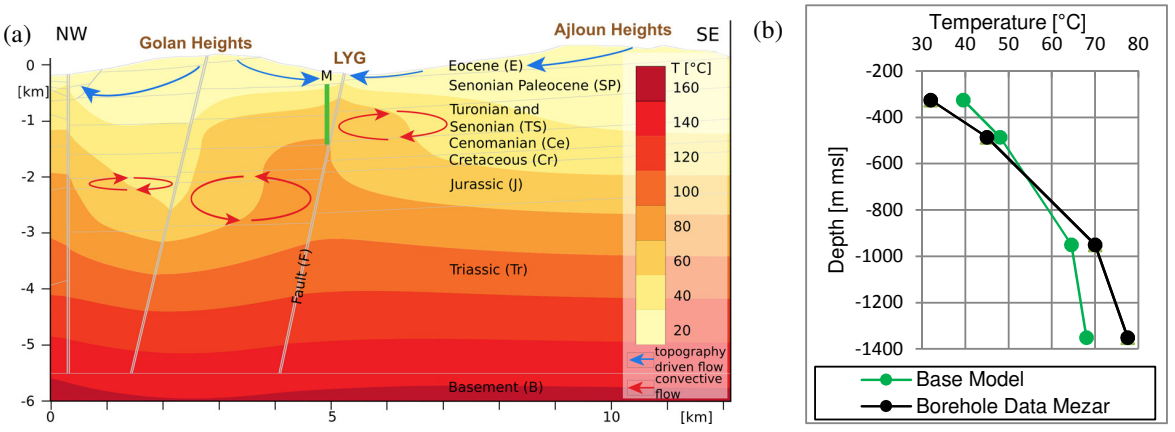

Fig. 4: Temperature profile (°C) obtained from numerical simulations of thermally-driven flow (forward problem) along a 2D vertical cross-section (modified after [4]). In this study, owing to the good temperature fit with the Meizar log data (M), this temperature plume is used in the inverse models (IP) to perform the automated calibration process.

In the shallow units, topography driven flow (blue arrows in Fig. 4a) dominates the fluid flow and pushes cooler water from Ajloun and Golan Heights towards the discharge areas (e.g. LYG). The deepest part of the profile (Jurassic and Basement) is characterized by conductive temperature flow. Below the LYG, buoyancy forces induce

heated water to rise in form of a thermal plume. The resulting flow generates large-scale (up to 2 km) convective cells (red arrows in Fig. 4a). The calculated temperature gradients within the Meizar wells are reproduced (Fig. 4b). However, calculated temperatures in the shallow (Eocene and Miocene) and in the deeper aquifers (Turonian) are up to 10 °C hotter and colder than the measured values, respectively.

The first IP (scenario 1) suggests that the SP aquitard is three times less permeable than assumed in the base model (Table 1). This finding is in good agreement with the findings from Mukheibeh wells in the LYG recently drilled by the Water Authority of Jordan, which show thick Senonian layers of almost impermeable chalks. The IP also predicts slightly less permeable faults and Jurassic unit than the FP.

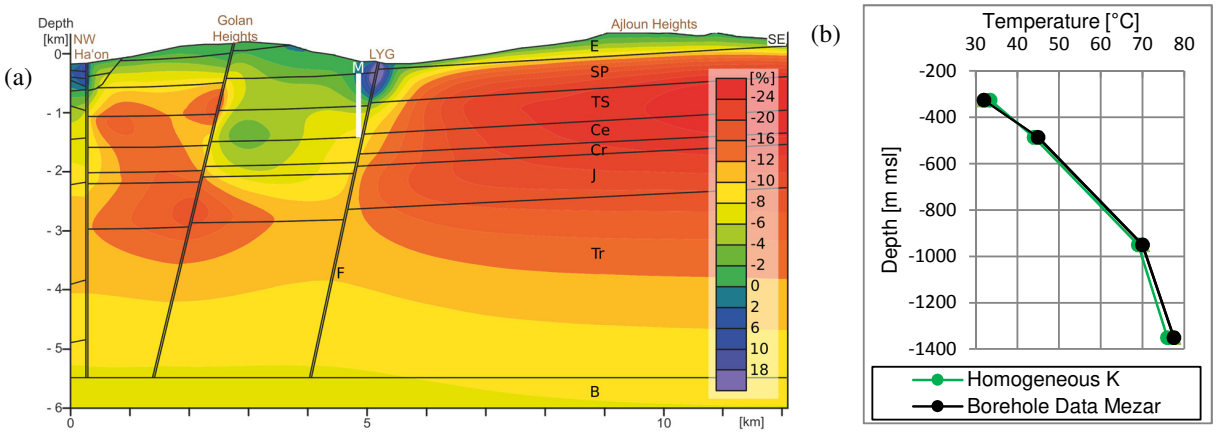

Fig. 5. (a): Temperature differences in percent between scenario 1 and scenario 2 with equation 2 and (b): Temperature-depth profile against Meizar well data.

Fig. 5a illustrates the relative temperature variation (equation 2) that is induced by the hydraulic conductivity distribution of the IP. The temperature variation (ΔT) is calculated with the following equation:

$$\Delta T = (T_{FP} - T_{IP1}) \div T_{FP} \times 100 \quad (2)$$

where T_{FP} is the temperature calculated with the base model and T_{IP1} is the temperature calculated with the IP (scenario 1).

Bluish and reddish areas indicate colder and warmer temperatures than those calculated with the FP, respectively. The local decreases in temperature observable at the discharge areas (Ha'on and LYG) nicely reflect the effects of SP as an aquiclude. Compared to the base model, the less permeable SP reduces upward flow of the thermal waters rising from below and the leakage of recharge water into deeper units. As a result, a larger volume of cold water from the Golan and Ajloun Heights is flushed through the LYG fault, leading to low temperature discharge. By contrast, since less heat is released through the top surface of the profile, an increase of temperature is predicted in the deeper units. Peak temperature differences occur in the southeastern part of the profile. However, results of the southeastern part are likely to be less accurate as few temperature observation points were defined (see Fig. 3). Overall, the hydraulic conductivity distribution inferred from this IP provides a very good fit of the simulated geothermal gradient with the Meizar well data (Fig. 5b).

In scenario 2, the hydraulic conductivity in the faults is allowed to be heterogeneous and optimized throughout the runs. The IP results (Fig. 6, Table 1) show that values in the units are higher than in the base model and scenario 1. The IP shows that at Triassic depths, the fault conductivity strongly decreases with a maximum estimated value of 0.04 m/d. A further decrease in fault permeability occurs in the LYG at Jurassic depths, to values close to that of the surrounding sediments (0.008 m/d), implying the absence of deep permeable pathways (Fig. 6a, zoom). Since in the previous scenario faults acted as the main pathways for the circulation of groundwater, mass balance

requires that the hydraulic conductivity of other zones increases in order to allow the same volume of water to flow, thereby preserving a good temperature fit. The IP identified those zones as the Cretaceous aquifer (1 m/d) and local areas of the LYG fault (0.2 m/d) at the intersection with the Turonian-Senonian aquifer. This scenario implies that the LYG temperature anomaly could also be caused by local structural weaknesses or anisotropic zones within a highly permeable Cretaceous aquifer. This finding is consistent to the presence of highly karstified Cretaceous sediments within this area.

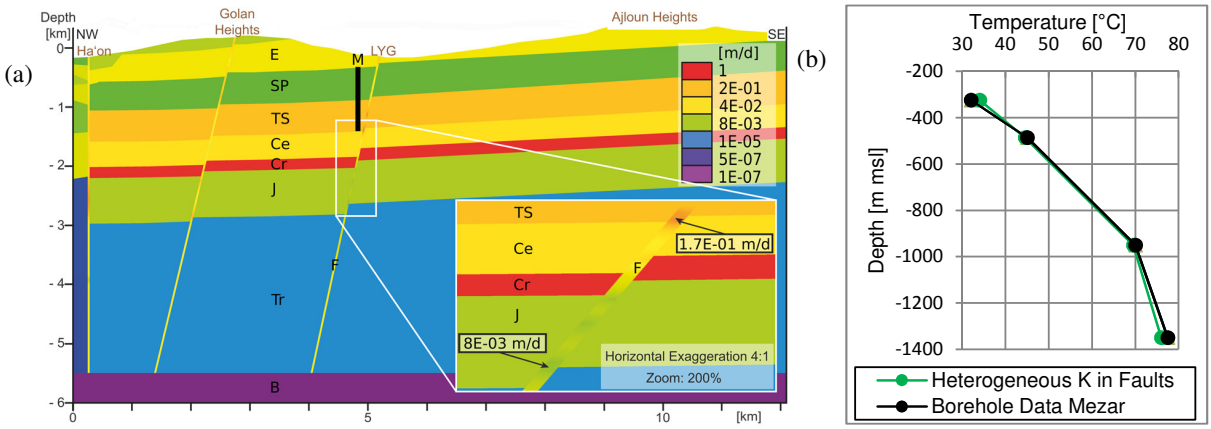

Fig. 6 (a) Scenario 2: Heterogeneous faults. Hydraulic conductivity values (m/d) in the faults are estimated using pilot points, while the surrounding units are zonally constant. (b) Temperature-depth profile against Meizar well data.

In a final scenario, the calibration focused on the thermal conductivity in order to assess the importance of the conductive regime on the temperature field. It turned out that this IP predicts thermal conductivity values several order of magnitudes higher than those encountered in sedimentary basins. This finding further highlights that heat conduction alone cannot induce the observed temperature anomalies of the LYG.

4. Conclusions

Forward problems of fluid flow and temperature log data indicate that the anomalous temperature gradient of the Lower Yarmouk Gorge (LYG) is likely due to a thermally-driven rising plume (Fig. 4). Inverse problems (IP) are applied to better constrain the hydraulic conductivity distributions in the basin. The IP suggests that the Senonian aquiclude is very impervious and strongly bounds shallow groundwater flow within Eocene sediments (Fig. 5). The IP predicts two major scenarios that shed light on the development of the observed LYG thermal anomaly: (i) Either outflow of thermal water occurs through relatively permeable and continuous faults reaching Triassic depths, or (ii) in the absence of a permeable pathway within Jurassic and deeper sediments, the increased temperature gradient within the LYG is due to local fractures interconnected by a highly permeable Cretaceous aquifer (Fig. 6). The contribution of the conductive thermal regime to the LYG anomaly is negligible with respect to density-driven flow.

Acknowledgements

The authors gratefully acknowledge the DFG – German Research Foundation - for funding this research within the framework of the trilateral program to support peaceful development in the Middle East (Grant DFG MA4450/2-3).

References

[1] Möller P, Siebert C, Geyer S, Inbar N, Rosenthal E, Flexer A, Zilberbrand M. Relationship of brines in the Kinnarot Basin, Jordan–Dead Sea Rift Valley. Geofluids 2012;12(2):166–181.
[2] Möller P, Rosenthal E, Flexer A. The hydrogeochemistry of subsurface brines in and west of the Jordan–Dead Sea Transform fault. Geofluids 2014;14(3):291–309.
[3] Bergelson G, Nativ R, Bein A. Assessment of hydraulic parameters of the aquifers around the Sea of Galilee. Ground Water 1998;36(3):409-417.
[4] Magri F, Inbar N, Siebert C, Rosenthal E, Guttman J, Möller P. Transient simulations of large–scale hydrogeological processes causing temperature and salinity anomalies in the Tiberias Basin. Journal of Hydrology 2015;520:342–355.
[5] Gvirtzman H, Garven G, Gvirtzman G. Hydrogeological modeling of the saline hot springs at the Sea of Galilee, Israel. Water Resources Research 1997;33(5):913–926.
[6] Gvirtzman H, Garven G, Gvirtzman G. Thermal anomalies associated with forced and free ground–water convection in the Dead Sea rift valley. Geological Society of America Bulletin 1997;109(9):1167–1176.
[7] Roded R, Shalev E, Katoshevski D. Basal heat–flow and hydrothermal regime at the Golan–Ajloun hydrological basins. Journal of Hydrology 2013;476:200–211.
[8] Levitte D, Olshina A, Wachs D. Geological and Geophysical Investigation in the Hammat Gadder Hot Springs Area Ministry of Energy and Infrastructure, Geological Survey of Israel, Hydrogeology and Environmental Geology Division; 1978.
[9] Siebert C, Möller P, Geyera S, Kraushaar S, Dulski P, Guttman J, Subah A, Rödiger T. Thermal waters in the Lower Yarmouk Gorge and their relation to surrounding aquifers. Chemie der Erde – Geochemistry 2014;74(3):425-441. doi:10.1016/j.chemer.2014.04.002.
[10] Ingebritsen SE, Gleeson T. Crustal permeability: Introduction to the special issue. Geofluids 2015;15:1-10. doi:10.1111/gfl.12118.
[11] Sagar B, Yakowitz S, Duckstein L. A direct method for the identification of the parameters of dynamic nonhomogeneous aquifers. Water Resources Research 1975;11 (4):563-570.
[12] Tarantola A. Inverse Problem Theory and Methods for Model Parameter estimation. SIAM: Society for Industrial and Applied Mathematics, 1st edition (December 20, 2004); 2005.
[13] Carrera J, Alcolea A, Medina A, Hidalgo J, Slooten L. Inverse problem in hydrogeology. Hydrogeology Journal 2005;13(1):206-222.
[14] Liu X, Kitanidis PK. Large-scale inverse modeling with an application in hydraulic tomography. Water Resources Research 2011;47(2):W02501.
[15] Irbar V, Carrera J, Custodio E, Medina A. Inverse modelling of seawater intrusion in the Llobregat delta deep aquifer. Journal of Hydrology 1997;198(1-4):226-244.
[16] Kool JB, Parker JC. Analysis of the inverse problem for transient unsaturated flow. Water Resources Research 1988;24(6):817-830.
[17] Diersch HJG. FEFLOW finite Element Modeling of Flow, Mass and Heat Transport in Porous and Fractured Media. Springer-Verlag Berlin Heidelberg; 2014.
[18] Doherty J. PEST® surface water modeling utilities: Numerical Computing, Watermark, Brisbane, Australia; 2007.
[19] Zhou H, Gómez-Hernández JJ, Li L. Inverse methods in hydrogeology: Evolution and recent trends. Advances in Water Resources 2014;63(0):22-37.